In situ prepared poly(ether-ester)-based gel polymer electrolytes for high-performance lithium metal batteries

Yang Chen,[a] Yin Zhang,[a] Weiguo Liang,[a] Hongli Xu,[b] Zhixian Dong,[a] Jinbao Xu,*[a] and Caihong Lei*[a]

1. Experiments

1.1 Materials

DXO was synthesized through Bayer-Villiger oxidation according to the literatures, and then purified by recrystallization from the dry ether, and two subsequent distillations under reduced pressure. [1, 2] Triethylamine (TEA, Sinopharm, 97%), toluene (Aladdin, 99%), stannous octoate ($Sn(Oct)_2$, Aladdin, 99%), chloroform ($CHCl_3$, Aladdin, 97%) were all dried over calcium hydride (CaH_2) and distilled prior to use. Acryloyl chloride (Aladdin, 96%) was obtained from Aladdin and distilled before use. Azodiisobutyronitrile (AIBN, Lingfeng chemical Co., Ltd., 99%) was recrystallized twice from dried n-hexane and stored at - 5 ℃. Pentaerythritol (Aladdin, 99%) was purified by two runs of sublimation prior to use. Cellulose membrane (NKK TF4030), polyvinylidene fluoride (PVDF, Canrd, weight-average molecular weight, M_w = 400 000 g mol^{-1}, 99%), $LiFePO_4$ (LFP, Macklin, battery-grade), super-P carbon black, $LiNi_{0.5}Co_{0.2}Mn_{0.3}O_2$ (NCM_{523}) (Canrd, battery-grade), 1 M solution of LE consisted by $LiPF_6$ and EC/DEC (1:1 in volume, Kejing, GC) and N-methyl-2-pyrrolidone (NMP, Aladdin, GC) were commercially obtained. Other reagents from Sinopharm or Sigma-Aldrich were used as received.

1.2 Characterizations

Proton nuclear magnetic resonance (^{1}H NMR) spectra were conducted on a Bruker AV400 NMR spectrometer by using deuterated chloroform ($CDCl_3$) as the solvent and tetramethylsilane (TMS) as the internal standard. Fourier-transform infrared (FT-IR) spectra were recorded on a FT-IR-Digilab FTS3100FTIR spectrometer with potassium bromide (KBr) pellet. The surface and cross-section morphologies of the films were observed by JEOL JSM-6700F scanning electron microscopy (SEM) after 60 seconds platinum sputtering. Thermogravimetric analysis (TGA) was performed on a TA SDT Q600 instrument under a nitrogen atmosphere at a heating rate of 10 ℃ min^{-1} in the range of 25 to 800 ℃.

The ionic conductivities of the new electrolytes were characterized by electrochemical impedance spectroscopy (EIS) on a VMP3B-10 electrochemical workstation at an AC amplitude of 10 mV with a frequency range from 1 MHz to 10 mHz. A stainless-steel sheet (SS) was used as the blocking electrode to carry out the EIS measurements and the ionic conductivity was calculated by equation (1):

$$\sigma = \frac{L}{R \times S} \quad (1)$$

where L, R, and S stand for the thickness of electrolytes, the impedance of the bulk electrolyte, and the contact area between the two stainless-steel sheets, respectively.

The lithium-ion transference number (t_{Li^+}) was characterized by chronoamperometry (VMP3B-10 electrochemical workstation) and the t_{Li^+} was calculated on the basis of equation (2):

$$t_{Li+} = \frac{I_s \times (\Delta V - I_0 \times R_0)}{I_0 \times (\Delta V - I_s \times R_s)} \quad (2)$$

where △V is the potential difference (10 mV), I_0 and I_s are the initial current and the steady-state current before and after polarization, respectively, while R_0 and R_s are the interfacial resistances before and after polarization.

The electrochemical stability window (ESW) of the electrolyte was measured by using linear sweep voltammograms (LSV) in a voltage range of 2 to 6 V (vs. Li/Li^+) at a scanning rate of 1 mV s^{-1} by using CR-2032 batteries of SS/GPE/Li.

The galvanostatic cycling measurement of Li/GPE/Li batteries was carried out on a CT-1008-S1 charge/discharge instrument (Neware) and all the batteries were cycled for 1 h of charge and the subsequent 1 h of discharge.

The cycling performance and rate capability of LFP/GPE/Li batteries (CR2032) were conducted on a battery test system (CT-1008-S1, Neware) under different potential ranging from 2.5 to 4.0 V at room temperature. Cycling performance of the NCM_{523}/GPE/Li batteries (CR2032) were measured with high-voltage from 3.0 to 4.3 V at room temperature.

1.3 Synthesis of vinyl-ended star-shaped PDXO-Ac precursor

1.3.1 Synthesis of star-shaped PDXO500 oligomer

One typical process for the ROP of DXO is carefully described in Scheme 1a: DXO (1.29 g, 12 mmol), pentaerythritol (0.40 g, 3 mmol) and $Sn(Oct)_2$ (1.21 g, 3 mmol) were added to a Schlenk reactor equipped with a magnetic stirrer in a glove box, and the reactor was bulk polymerized at 130 ℃. The polymerization was quenched by the addition of a few drops of acetic acid after 3 h. The product was diluted with THF and poured into a large excess of cold ether to precipitate the polymer, which was then dried under vacuum. Yield: 1.62 g (96%). The number-average molecular weight (M_n) of the synthesized oligomer was calculated on the basis of ^{1}H NMR spectrum (M_n = 590 g mol^{-1}, which was defined as PDXO500).

1.3.2 Synthesis of double bond-ended four-armed PDXO-Ac precursor

PDXO500 (6.50 g, 13 mmol) was dissolved in 50 mL of chloroform in a glass vessel and then TEA (2.63 g, 26 mmol) was added under 0 ℃. After the dropwise addition of the solution of acryloyl chloride (2.35 g, 26 mmol) in 20 mL of chloroform at this temperature over 2 h, the mixture was allowed to stir at room temperature for another 20 h. The precipitated triethylamine hydrochloride was filtered out and the solvent was removed under vacuum. The obtained product was dissolved in dichloromethane and poured into a large excess of a n-hexane/ether mixture (90/10 by volume) to precipitate the polymer, which was then dried under vacuum. Yield: 7.36 g (92%). ^{1}H NMR analysis shows that the M_n of the obtained precursor is 650 g mol^{-1} (double bond-ended four-armed PDXO was designated as PDXO-Ac).

1.4 Synthesis of PDXO-based cross-linked GPE

Regarding the straightforward way to prepare *in situ* polymerized GPE in facile preparation process with reduced interface impedance and good compatibility between electrolyte and electrode mentioned in an army of publications, which facilitates the performance improvement of LIBs, the *in situ* GPEs are more suitable for large-scale application. However, the typical disadvantage for in situ GPE separators is the inquires of initiator, heat or other external conditions while some initiators may affect the battery performance. For *ex situ* GPE separators (generally prepared by the solution casting method), the advantages are the controllable preparation process and little influence by external conditions while the disadvantages are the cumbersome preparation process (more suitable for lab-scale), poor compatibility between electrolyte and electrode (poor performance of LIBs), and organic solvents pollute the environment this. In this context, the ex-situ GPE separators are more suitable for lab studies. Having this in mind, the *in situ* polymerization method was chosen to fabricate high performance LIBs for scientific investigations though it is more suitable for large-scale application.

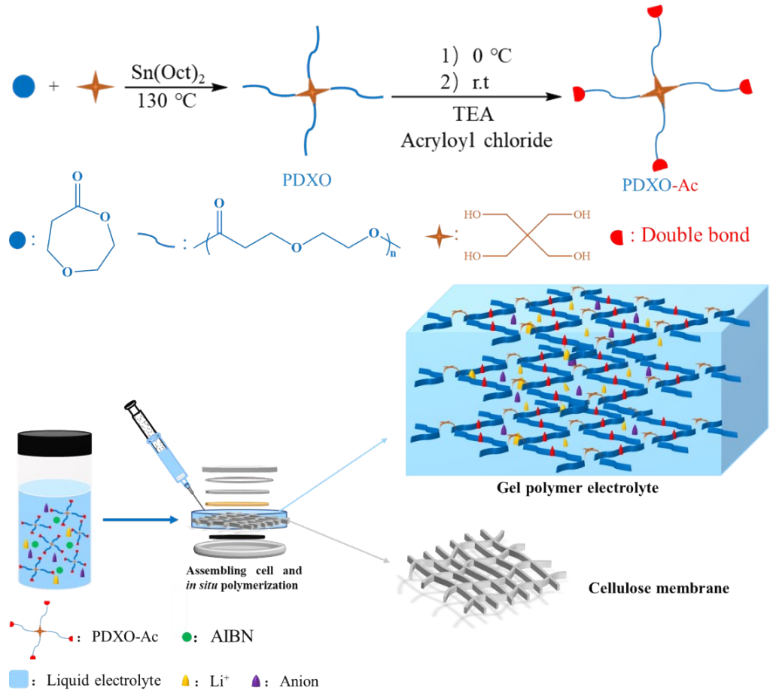

Scheme S1. Schematic illustration of the preparation of (a) the PDXO500 oligomer and PDXO-Ac precursor; (b) the PDXO-based cross-linked GPE.

Considering the polymerizable precursor in our material box, *in situ* polymerization was used to fabricate the PDXO-based GPEs via traditional thermal-induced radical polymerization of the acrylate-terminated PDXO-Ac precursor in the presence of LE (Scheme S1b; the polymerization mechanism is illustrated in Fig. S1). It is well known that the

mechanical strength of a gel is usually lower than that of a solid, and thus a supporter is generally needed for GPE-based LIBs.[3] Consequently, a cellulose membrane (stable enough in the LE) with a pore size of 0.8–3 μm (benefiting the transmission of the active electrode) was selected as a support to improve the mechanical properties and thermal stability of the composites (cellulose membrane and polymer electrolytes). The transformation of the original white cellulose membrane (Fig. S2a) into a translucent light-yellow one (Fig. S2b) also indicates the successful *in situ* polymerization of PDXO-Ac in the pores of the membrane. Moreover, the thickness of the cellulose membrane–supported PCG (PDXO-Ac based cross-linked GPE and cellulose membrane) is about 50 ± 5 μm, which could be easily regulated based on the contents of the injected PDXO-Ac precursor mixture.

The preparation of PDXO-based cross-linked GPE is presented in Scheme 1b. Typically, PDXO-Ac (0.5 g, 5 wt% to the LE), LE (10.0 g) and AIBN (10.0 mg) were mixed under stirring (6 h) to give a homogeneous mixture. The homogeneous mixture (60 μl) was then injected into the cellulose membrane (supporting skeleton, the diameter is 1.6 cm); subsequently, the supporting membrane was sealed in a cell between the electrodes followed by heating at 60 ℃ for 24 h to complete the *in situ* polymerization (the thickness of the cellulose membrane-supported PCG is about 50 ± 5 μm and the area is 2.0 cm^2). In comparison, the cellulose membrane injected with the homogenous mixture was placed between two pieces of PTFE plates and heated at 60 ℃ for 24 h to obtain the *ex situ* GPE; then, the membrane was peeled off from the PTFE plates and also used as the supporting to batteries. In order to accurately control the composition of LE and make the influence of that in a negligible level, the GPEs were prepared in an oven (2 L) with a cup of LE near the GPEs. All procedures were carried out in an Ar-filled glove box with the contents of oxygen and moisture < 0.01 ppm. Other samples were prepared in a similar way and the PDXO-Ac -based cross-linked GPE was defined as PCGX%, where the "X%" depicts the weight fraction of PDXO-Ac to the LEs.

1.5 Preparation of LFP and NCM_{523} cathodes

The LFP cathode was prepared with a conventional casting method: LFP (0.8 g) active particles, super-P (0.1 g) and PVDF binder (0.1 g) were dispersed in NMP solvent, which was then uniformly coated on an aluminum foil by a scraper blade. After that, the cathode was kept at 60 ℃ under vacuum for 72 h to remove the residual solvent. The area specific density of the LFP was about 2.5 mg cm^{-2}. Similarly, NCM_{523} cathode was prepared and the area specific density was about 2.0 mg cm^{-2}

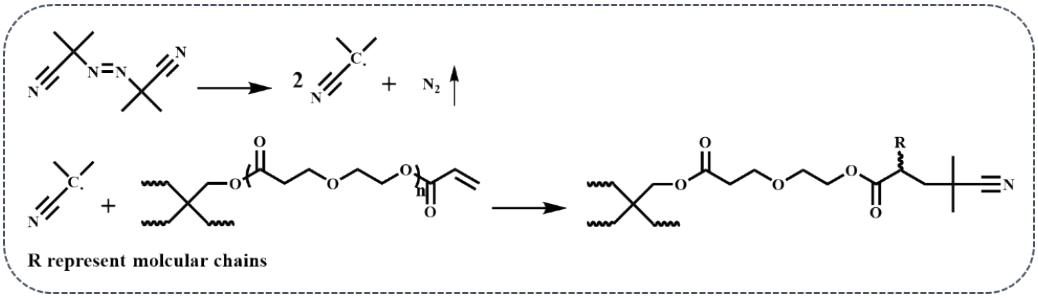

Fig. S1. Polymerization mechanism of acrylate functionalization of four-armed PDXO500.

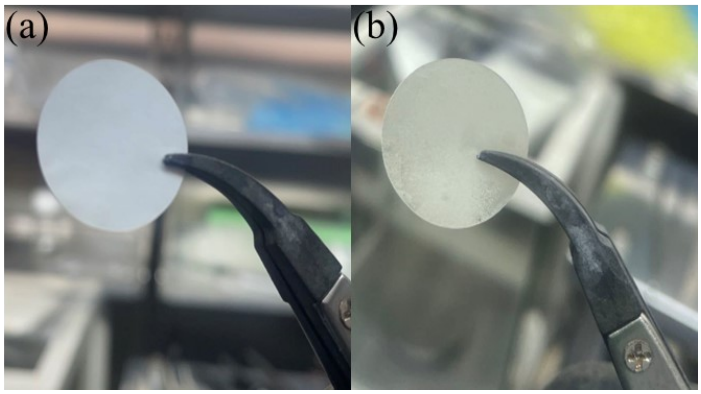

Fig. S2. Digital photographs of (a) original cellulose membrane and (b) cellulose membrane-supported PCG.

To further survey the morphology and structural changes of the membrane-supported PCG composite after *in situ* polymerization, SEM characterization was employed to outline the surface and cross-sectional images. As shown in Fig. S3(a and c), the pores of the original cellulose membrane are arranged randomly, whereas the pores are filled with crosslinked PDXO-based polymers after in situ polymerization, and a dense and continuous morphology of the PCG composite can be observed (Fig. S3b). In addition, the cross-sectional image shows that the *in situ*-generated PCG is uniformly incorporated into the pores of the cellulose membrane to form continuous channels, ensuring a continuous transport path for lithium ions, blocking the growth of lithium dendrites and preventing micro-short circuiting (Fig. S3d). However, the fabricated LFP electrode exhibits an uneven surface and is coated with a layer of polymer electrolyte (Fig. S4(a and c)), which is attributed to the *in situ* cross-linked polymerization of the PDXO-Ac precursor. Attractively, the composite membrane is still closely adhered to the LFP electrode after 50 cycles (Fig. S4(b and d)), once again revealing the advantage of the *in situ* polymerization process, which can greatly improve the compatibility of the electrolyte and electrode, thus decreasing the interfacial resistance.

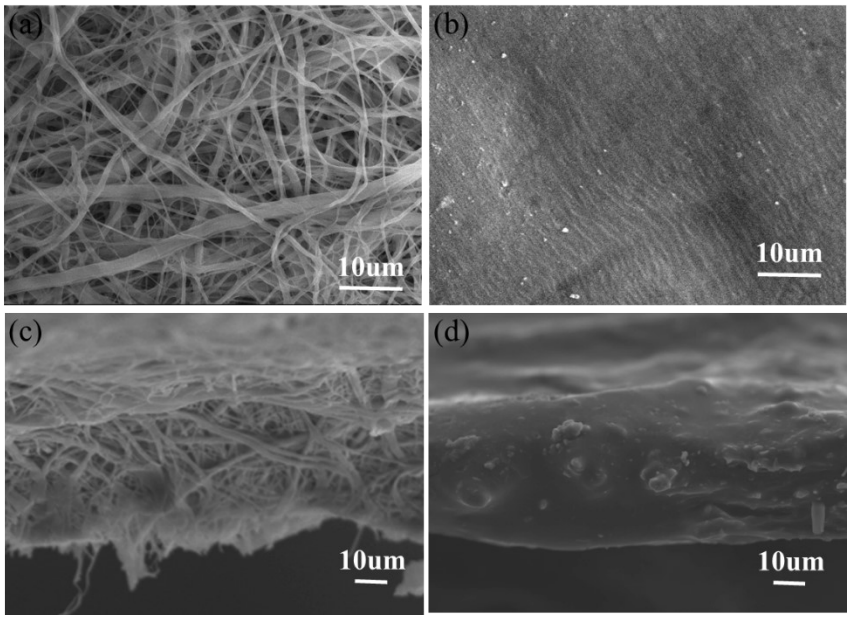

Fig. S3. Typical SEM images of (a) surface and (c) cross-section of the original cellulose membrane; (b) surface and (d) cross-section of the composite membrane after *in situ* polymerization.

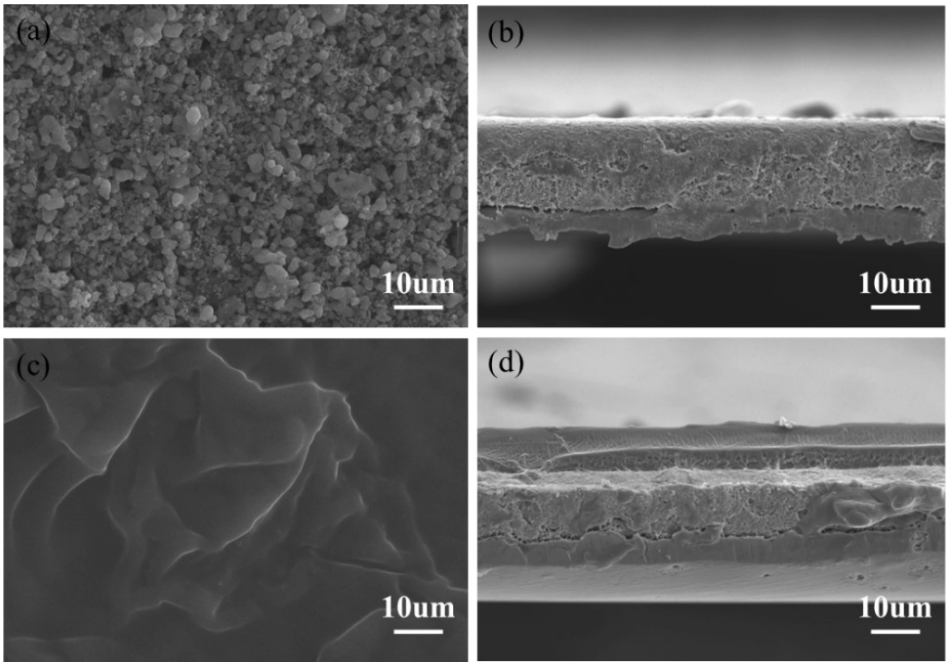

Fig. S4. Typical SEM images of (a) the surface and (b) cross-section of original $LiFePO_4$ electrode; (c) the surface and (d) cross-section of $LiFePO_4$ electrode after 50 cycles and.

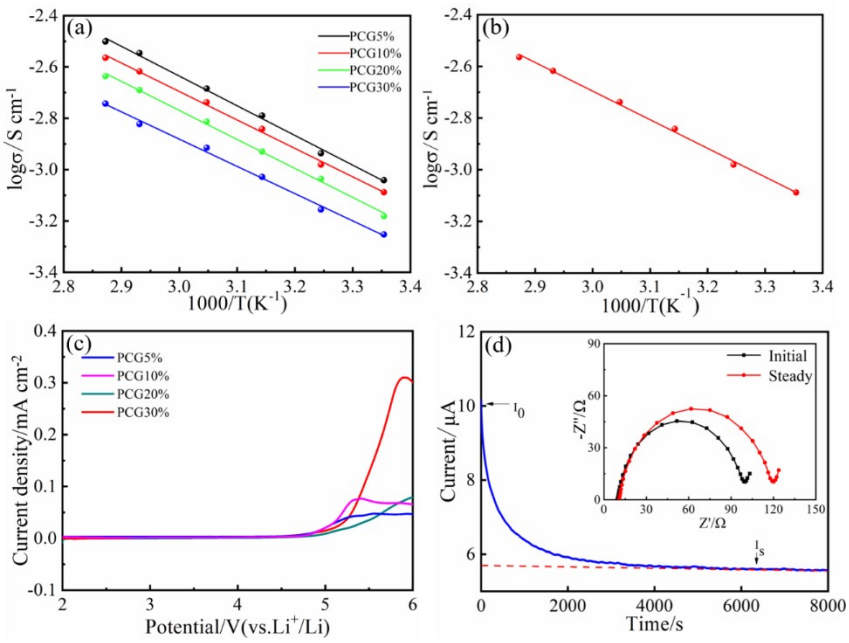

Fig. S5. Electrochemical performance of PCG: (a) Arrhenius plot of ionic conductivity of the PCG; (b) Arrhenius plot of ionic conductivity for PCG10%; (c) LSV of PCG; (d) the chronoamperometry curves of the symmetric Li|PCG|Li battery with a DC polarization of 10 mV (inset is the Nyquist plots before and after the polarization).

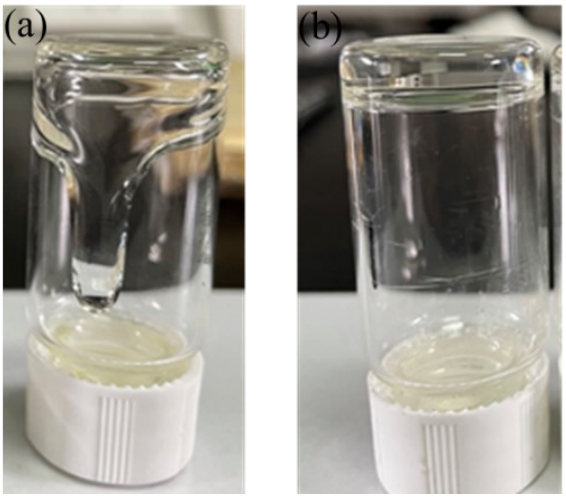

Fig. S6. Digital photographs of the samples after crosslinking reaction with different contents of PDXO-AC precursor (a) 5% and (b) 10%.

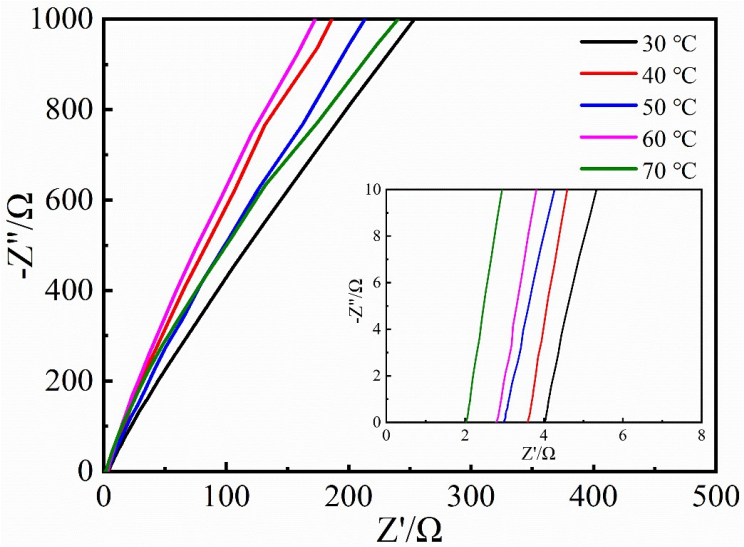

Fig. S7. The AC impedance spectra of PCG10% at different temperatures.

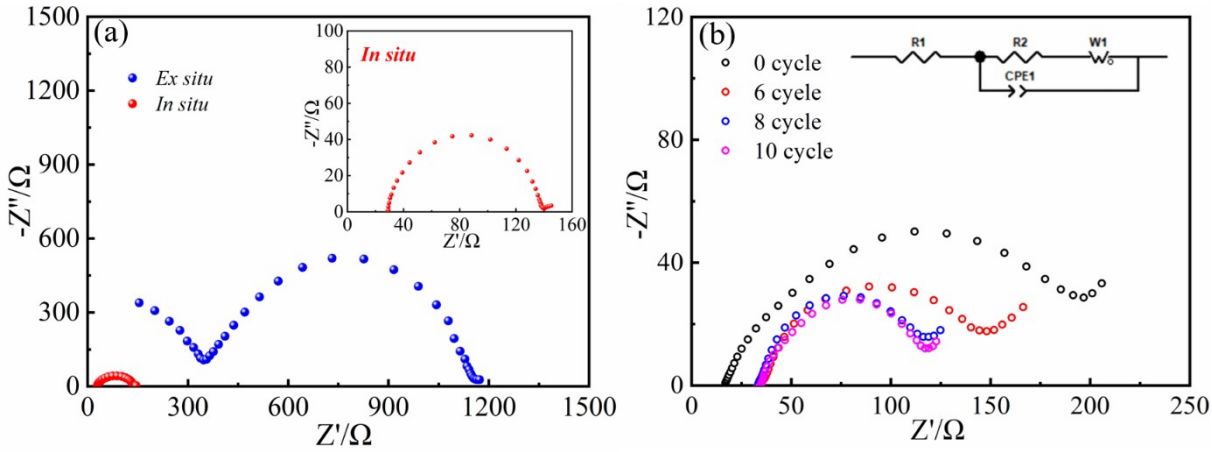

Fig. S8. (a) EIS impedance spectra of *in situ* and *ex situ* prepared Li/PCG/Li batteries at room temperature; (b) EIS impedance spectra of *in situ* prepared LFP/PCG/Li battery after different cycles at room temperature.

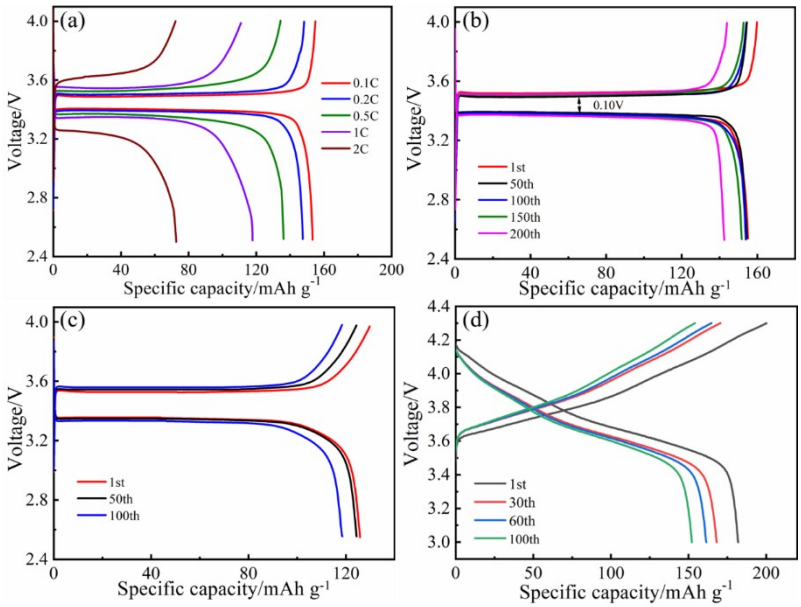

Fig. S9. (a) charge-discharge voltage profiles of the LFP|PCG|Li batteries from 0.1 C to 2 C; (b) charge-discharge voltage profiles of the LFP|PCG|Li batteries at 0.2 C in the 1st, 50th, 100th, 150th and 200th cycle and (c) at 1.0 C in the 1st, 50th and100th cycle at room temperature;(d) charge-discharge voltage profiles of the NCM_{523}|PCG|Li battery at 0.1 C in the 1st, 30th, 60th and 100th cycle.

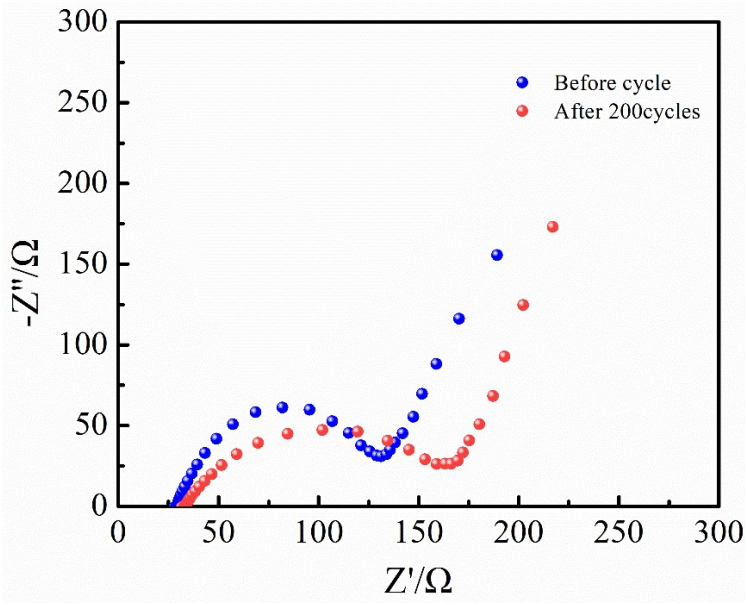

Figure S10. EIS impedance spectra of the LFP/PCG/Li batteries before and after 200 cycles.

References

[1] T. Mathisen, A.C. Albertsson, *Macromolecules*, 1989, **10**, 3838-3842.
[2] T. Mathisen, K. Masus, A.C. Albertsson, *Macromolecules*, 1989, **10**, 3842-3846.
[3] M. Zhu, J. Wu, Y. Wang, M. Song, L. Long, S. H. Siya, X. Yang, G. Sui, *J. Energy Chem.*, 2019, **37**, 126-142.